Scripta Materialia 148 (2018) 10–14

Contents lists available at ScienceDirect

Scripta Materialia

journal homepage: www.elsevier.com/locate/scriptamat

Regular article

# Compressive creep behavior of hot-pressed $Mg_{1.96}Al_{0.04}Si_{0.97}Bi_{0.03}$

Richard A. Michi [a], Gwansik Kim [b], Byung-Wook Kim [c], Wooyoung Lee [b,*], David C. Dunand [a,*]

[a] Department of Materials Science and Engineering, Northwestern University, 2220 Campus Drive, Evanston, IL 60208-3108, USA
[b] Department of Materials Science and Engineering, Yonsei University, Seoul 03722, Republic of Korea
[c] Advanced Materials Research Team, Hyundai Motor Company, Uiwang 16082, Republic of Korea

ARTICLE INFO

*Article history:*
Received 19 December 2017
Received in revised form 9 January 2018
Accepted 9 January 2018
Available online 30 January 2018

*Keywords:*
Creep
Thermoelectric materials
Silicides
Hot pressing
Magnesium silicide

ABSTRACT

The compressive creep behavior of hot-pressed $Mg_{1.96}Al_{0.04}Si_{0.97}Bi_{0.03}$, a promising thermoelectric material, is investigated at 500 °C. At stress levels between 81 and 212 MPa, dislocation creep with stress exponent $n = 7.6 \pm 0.3$ is observed. No diffusional creep is observed, likely attributable to a dispersion of ~1 μm Bi-, Al-, and O- rich particles which pin grain boundaries. $Mg_{1.96}Al_{0.04}Si_{0.97}Bi_{0.03}$ exhibits similar creep behavior to previously studied silicides, but is significantly more creep resistant than other thermoelectric materials, PbTe and $Bi_2Te_3$. This makes $Mg_{1.96}Al_{0.04}Si_{0.97}Bi_{0.03}$ an excellent material for thermoelectric power generation systems subjected to high stresses and temperatures.



Thermoelectric generators (TEG's) harness the properties of thermoelectric materials by converting thermal energy into electrical energy [1]. TEG's can be used to convert the waste heat from internal combustion engines [2–4] or industrial processes [5,6] into useful electrical power. During the operation of TEG's, the thermoelectric material can be subjected, for very long times, to significant thermal stresses due to the temperature differences between the hot and cold side of the device, mechanical forces due to the clamping forces used to secure the materials, and vibrations from operation, e.g., in automotive applications [7,8]. In addition, these devices often operate at high homologous temperatures ($T_H = T/T_m$, where $T_m$ is the melting point of the thermoelectric material), leading to potentially significant creep deformation over long periods of operation. Therefore, the mechanical properties, including the creep resistance, of the thermoelectric material are of interest when designing reliable TEG's.

Recently, $Mg_2Si$ doped with Bi and Al to a composition $Mg_{1.96}Al_{0.04}Si_{0.97}Bi_{0.03}$ has been identified as a promising thermoelectric material owing to the abundance and nontoxicity of its constituent elements, low density (2.05–2.1 g $cm^{-3}$), and ZT value of 1.02 [9,10]. The thermoelectric properties have been evaluated from 127 to 627 °C, with the latter temperature at the high end of the likely operating temperature range, corresponding to $T_H = 0.66$ (given the melting temperature of pure $Mg_2Si$ of 1090 °C [11]), well within the creep regime [12]. The melting temperature of $Mg_{1.96}Al_{0.04}Si_{0.97}Bi_{0.03}$ is expected to be similar to that of pure $Mg_2Si$, as the Al and Bi dopant concentrations are low. The crystal structure of $Mg_2Si$ is of the antifluorite type, with an FCC cubic lattice [13]. The bonding nature of pure $Mg_2Si$ is mostly covalent, with an ionicity of 8% [14]. This leads to the brittle behavior and low fracture toughness observed in $Mg_2Si$ and $Mg_{1.96}Al_{0.04}Si_{0.97}Bi_{0.03}$ [15,16]. However, the material may exhibit more ductile behavior at high $T_H$.

The creep properties of thermoelectric materials have not been widely studied and those of $Mg_{1.96}Al_{0.04}Si_{0.97}Bi_{0.03}$ are unknown. Compressive creep of coarse-grained $Bi_2Te_3$ was measured at stress ranges of 2–16 MPa and temperature ranges of 400–500 °C ($T_H = 0.78$–$0.90$), exhibiting power-law dislocation creep behavior across all temperatures. The material behaved in a brittle manner between 400 and 450 °C, and exhibited anisotropic creep resistance [17]. The creep properties of PbTe exhibiting a bimodal grain size distribution were evaluated at stress ranges of 2–35 MPa and temperature ranges of 350–500 °C ($T_H = 0.52$–$0.65$), exhibiting diffusional creep at stresses below ~8 MPa and dislocation creep at higher stresses. The material exhibited ductility across all test temperatures [18].

In this study, the compressive creep behavior of hot pressed $Mg_{1.96}Al_{0.04}Si_{0.97}Bi_{0.03}$ is evaluated at 500 °C ($T_H = 0.56$). The likely creep mechanisms are discussed according to the measured power-law creep behavior. The creep resistance is compared to those of the two previously studied thermoelectric materials (PbTe and $Bi_2Te_3$) as well as structural silicides whose behavior is expected to be similar (i.e. isomechanical) at the same homologous temperature, based on crystal structures and bonding [12].

$Mg_{1.96}Al_{0.04}Si_{0.97}Bi_{0.03}$ powders were prepared by solid state reaction as described in a previous study [10]. Polycrystalline samples (25 mm in diameter and 6 mm in thickness) were densified via hot pressing

* Corresponding authors.
*E-mail addresses:* wooyoung@yonsei.ac.kr (W. Lee), dunand@northwestern.edu (D.C. Dunand).

https://doi.org/10.1016/j.scriptamat.2018.01.011
1359-6462/

at 750 °C for 1 h under 70 MPa, resulting in densities between 97 and 99% of the theoretical density.

Creep samples were cut into 6.3 × 5.8 × 13.1 mm tetragonal prisms using a low speed diamond saw. The samples were placed between two tungsten carbide platens lubricated with boron nitride and heated in a three-zone furnace with thermal fluctuations of ±1.5 °C. Compressive stresses were applied to the samples using a Ni-base superalloy compression cage and hanging dead loads. Sample displacement was measured using a linear variable displacement transducer (LVDT). When a steady-state strain rate was achieved for a given stress as measured from the slope of the strain vs. time curve, the load was increased to obtain an additional steady-state strain rate. Thus, a single specimen provided several minimum strain rate vs. stress data points. Testing was terminated when the strain of the samples reached 10%.

Samples were polished to a 0.3 μm finish using standard metallographic procedures. Polished cross-sections were examined using a Hitachi SU8030 SEM, equipped with an Oxford X-max 80 mm detector for energy-dispersive x-ray spectroscopy (EDS) measurements. EDS mapping was performed using AZtec Energy software. One sample each was examined for the as-pressed and crept conditions.

Fig. 1a shows a representative SEM image of the as-pressed microstructure of the $Mg_{1.96}Al_{0.04}Si_{0.97}Bi_{0.03}$ material. The material consists of ~20–30 μm diameter densified regions surrounded by partially-densified regions containing ~1–10 μm diameter grains. In addition, ~20–50 μm diameter particles, labeled (i), (ii), and (iii) in Fig. 1a were observed. EDS analysis shows that particles (i) and (iii) are rich in Bi, Al, and O, and particle (ii) is rich in Bi and O. These particles are likely oxides that may have formed during the processing of the powders and their densification. Fig. 1b shows detail of the microstructure. The large ~20–30 μm densified regions appear to be composed of several grains roughly 10 μm in diameter, probably resulting from powder particles that were consolidated by hot pressing. In the partially-densified regions between the large ~20–30 μm densified regions, the ~1–10 μm grains appear to be composed of a mixture of partially-sintered powder particles. Regions of bright contrast, highlighted with arrows in Fig. 1b, are evident among the distribution of ~1–10 μm grains. The bright contrast suggests concentrations of the higher Z doping elements Al and Bi, which was confirmed by EDS mapping. EDS mapping revealed that the regions are also rich in O. These regions of bright contrast are likely due to Bi- and Al-rich oxides, similar to particles (i), (ii), and (iii) in Fig. 1a, but smaller. Fig. 1c and d show, respectively, optical micrographs of the as-pressed microstructure and microstructure after creep at 500 °C for 300 h. The apparent grain size does not change, and can be considered constant for the duration of the creep test.

Fig. 2a shows a plot of strain vs. time for the creep test performed at 500 °C. The primary creep regime, identified as the initial region of decreasing strain rate, extends to approximately 110 h at the first stress of 81 MPa and accounts for ~1% total strain. The primary creep regime is associated with the establishment of a steady-state dislocation structure within grains and at grain boundaries. In the secondary creep regime, a minimum strain rate is obtained for each applied stress. The resulting plot of minimum strain rate vs. applied stress is shown in Fig. 2b. The data in Fig. 2b can described by a power law creep equation [12]:

$$\dot{\varepsilon} = A\sigma^n \exp\left(-\frac{Q}{R_g T}\right) \quad (1)$$

where $\dot{\varepsilon}$ is the minimum secondary strain rate, $A$ is a constant, $\sigma$ is the applied stress, $n$ is the stress exponent, $Q$ is the activation energy for creep, $R_g$ is the gas constant, and $T$ is the absolute temperature. A stress exponent $n = 7.6 \pm 0.3$ was calculated using a power law fit of all points in Fig. 2b except for the highest stress of 230 MPa. The value of the stress exponent is indicative of a dislocation creep mechanism. Compared with other covalently bonded solids such as Si and Ge

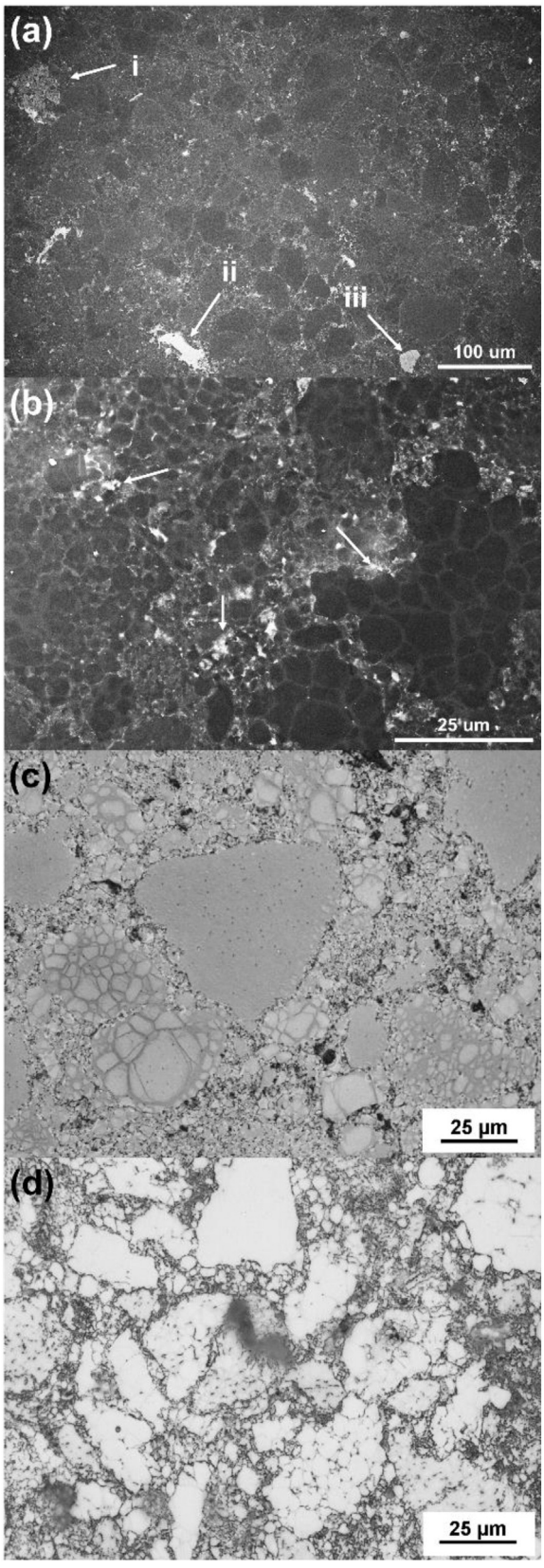


**Fig. 1.** (a–b) SEM micrographs showing polished cross-sections of as-pressed $Mg_{1.96}Al_{0.04}Si_{0.97}Bi_{0.03}$, displaying a mixture of densified and partially-densified regions, showing respectively, 10 μm grains and a distribution of ~1–10 μm grains. Bi-, Al-, and O-rich particles are highlighted with arrows in (a), Bi-, and Al-rich regions are highlighted in (b). (c–d) Optical micrographs of polished cross-sections of (c) as-pressed and (d) crept samples of $Mg_{1.96}Al_{0.04}Si_{0.97}Bi_{0.03}$, after 300 h at 500 °C and 81 to 230 MPa. The grain size does not change after creep.

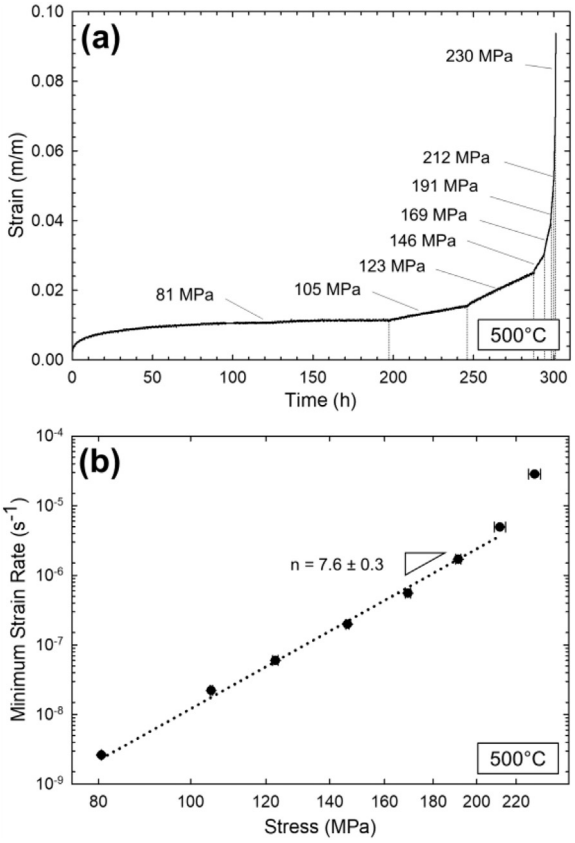


**Fig. 2.** (a) Plot of strain vs. time for compressive creep test performed at 500 °C for a series of increasing applied stresses, and (b) corresponding plot of minimum strain rates vs. stress, with value of the stress exponent n shown.

which have $n = 5$, our measured $n$ is higher, likely due to the differing crystal structure [12].

Diffusional creep does not appear to be active in $Mg_{1.96}Al_{0.04}Si_{0.97}Bi_{0.03}$ at the stress levels and temperature used here, as there is no region in Fig. 2b where $n = 1$. This is unusual, considering the presence of small ~1–10 μm grains that are expected to be prone to diffusional creep. The presence of small ~1 μm particles rich in Bi, Al, and O as highlighted in Fig. 1b may pin grain boundaries, preventing grain boundary sliding and thus effectively suppressing diffusional creep.

After creep testing at 500 °C, the crept sample exhibited signs of plastic deformation as well as cracking. Cracking is the likely cause for deviation of the point at 230 MPa from the best-fit line in Fig. 2b. The presence of cracks suggests that the material would have likely failed catastrophically had the sample been tested at stresses exceeding 230 MPa. During tests at 400 and 525 °C for which no steady-state strain rate could be achieved, the samples failed catastrophically after deforming 2.30 and 5.79% at 156 and 123 MPa, respectively. As the $Mg_{1.96}Al_{0.04}Si_{0.97}Bi_{0.03}$ catastrophically failed at 400 and 525 °C but not 500 °C, it is likely that brittle failure is highly sensitive to pre-existing flaws in the material at those relatively high stresses.

Structural silicides exhibit inherent brittleness due to their low degree of crystal symmetry, low number of independent slip systems, and high degree of directionality in the metal-Si bonds [19]. These factors also lead to relatively high ductile to brittle transition temperatures (DBTT) that often exceed $0.5T_m$. For polycrystalline $Cr_3Si$, whose cubic crystal structure and high degree of covalent bonding closely match $Mg_2Si$ [13,14,20,21], the DBTT is at $0.72T_m$ [19]. Thus, based on the observations in the current study, it is likely that the creep test temperatures of 400, 500, and 525 °C are all below the DBTT of $Mg_{1.96}Al_{0.04}Si_{0.97}Bi_{0.03}$.

Fig. 3a shows a plot of minimum strain rate vs. stress for the $Mg_{1.96}Al_{0.04}Si_{0.97}Bi_{0.03}$ tested in this study (data from Fig. 2b), along with previously studied thermoelectric materials (PbTe and $Bi_2Te_3$) and other silicides ($MoSi_2$,$V_3Si$, $Cr_3Si$, $TiSi_2$, $Mo_5Si_3$, $Ti_5Si_3$, and $Nb_5Si_3$), with test temperatures and grain sizes for each test given in the curve labels [17, 18, 22–26]. Fig. 3b shows the same data and the homologous temperature $T_H$ for each test, with stress values normalized by the room temperature Young's Modulus (E). Compared with the other two thermoelectric materials for which creep data are available, $Mg_{1.96}Al_{0.04}Si_{0.97}Bi_{0.03}$ is much more creep resistant at 500 °C, with measurable creep commencing at stresses about ten times higher than $Bi_2Te_3$ (at 500 °C) and PbTe (at 400 °C). When normalized to the Young's modulus of the materials, $Mg_{1.96}Al_{0.04}Si_{0.97}Bi_{0.03}$ maintains its superior creep resistance, making it an attractive thermoelectric material in applications where high stresses and temperatures and long creep times are encountered. The significant difference in high temperature strength among these thermoelectric materials is likely due to their differing bonding. Bonding in $Mg_2Si$ is 8% ionic (mostly covalent), thus it is expected to be highly creep resistant [12,14]. Bonding in PbTe is 88% ionic [27], therefore it is expected to be less creep resistant than $Mg_2Si$. $Bi_2Te_3$ exhibits mixed bonding, with ionic and covalent behavior within five-atom layers of Bi and Te, and Van der Waals bonding between these layers [28]. The presence of the ionic behavior and especially the weak Van der Waals bonding lead to much lower creep resistance compared to $Mg_2Si$.

$Mg_{1.96}Al_{0.04}Si_{0.97}Bi_{0.03}$ deforms at similar rates as the other silicides tested at similar stresses and values of $T_H$, ($Mo_5Si_3$, and $Ti_5Si_3$) although the value of the stress exponent n is higher, likely due to differences in crystal structure. $Mo_5Si_3$ and $Ti_5Si_3$ have body-centered tetragonal and hexagonal crystal structures, respectively, whereas $Mg_2Si$ has a cubic crystal structure [14,19]. The number of independent slip systems is smaller in the former structures, therefore the dislocation creep mechanism and the value of $n$ are expected to differ for these materials when compared to $Mg_2Si$. Both $Cr_3Si$ and $V_3Si$ have a cubic crystal structure with primarily covalent bonding [20,21], as does $Mg_2Si$. If these materials were crept at the same stresses but at lower $T_H$, similar to the $T_H$ used in this study, the curves for $Cr_3Si$ and $V_3Si$ shown in Fig. 3a would shift to lower strain rates, falling more closely in line with the creep results for $Mg_{1.96}Al_{0.04}Si_{0.97}Bi_{0.03}$, which has a similar crystal structure and bonding. With stress normalized to the Young's modulus, the creep curves for the silicides roughly group together in regions depending on the homologous temperatures of the tests, as shown by the shaded regions in Fig. 3b. Within the low $T_H$ region, $Mg_{1.96}Al_{0.04}Si_{0.97}Bi_{0.03}$ exhibits a creep resistance superior to $Mo_5Si_3$, similar to $Ti_5Si_3$, but slightly lower than $Nb_5Si_3$.

The 1–10 μm grain size of the studied $Mg_{1.96}Al_{0.04}Si_{0.97}Bi_{0.03}$ is the smallest of all shown silicide data, yet it does not appear to adversely affect its creep resistance (the grain size pertaining to the $Mo_5Si_3$ data is unknown). This is unexpected, as the creep resistance of structural silicides, particularly $MoSi_2$, has been shown to be highly sensitive to grain size [19]. For example, by increasing the grain size of $Mo_2Si$ from 4 to 25 μm, its minimum creep rate can be reduced from $6 \times 10^{-5}$ to $1 \times 10^{-8}$ $s^{-1}$ at 1200 °C ($T_H = 0.64$) for a 78 MPa applied stress [25]. The dispersion of ~1 μm Bi-, Al-, and O-rich particles observed in the microstructure of $Mg_{1.96}Al_{0.04}Si_{0.97}Bi_{0.03}$ likely pins grain boundaries and prevents grain boundary sliding, maintaining good creep resistance even for small 1–10 μm grains. This suggests that the current processing methods for $Mg_{1.96}Al_{0.04}Si_{0.97}Bi_{0.03}$ are capable of manufacturing material with high creep resistance.

This study examines the compressive creep behavior of hot-pressed $Mg_{1.96}Al_{0.04}Si_{0.97}Bi_{0.03}$. The material has a complex microstructure, with ~20–30 μm diameter densified regions composed of grains with ~10 μm diameter, surrounded by partially-densified regions of 1–10 μm grains which are likely a mixture of partially-sintered powder particles. There is no evidence of grain growth after creep at 500 °C for 300 h. At 500 °C under applied stresses between 81 and 212 MPa, the material

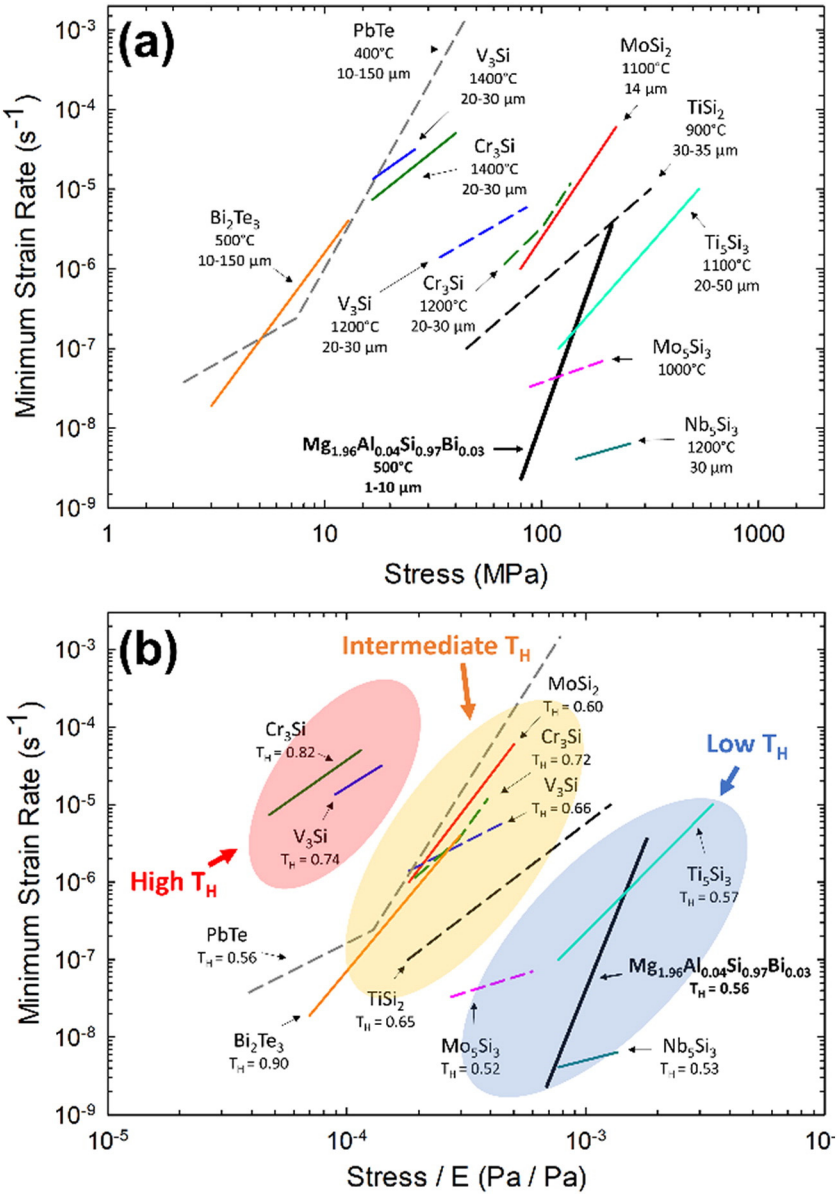


**Fig. 3.** (a) Plot of minimum strain rate vs. stress for the $Mg_{1.96}Al_{0.04}Si_{0.97}Bi_{0.03}$ along with literature data for other silicides, $V_3Si$, $Cr_3Si$, $TiSi_2$, $MoSi_2$, $Mo_5Si_3$, $Nb_5Si_3$, and $Ti_5Si_3$ (Refs. 22–26), and thermoelectric materials, PbTe and $Bi_2Te_3$ (Refs. 17–18). Creep temperatures and grain sizes are shown for each curve. (b) Plot of minimum strain rate vs stress normalized to the room-temperature Young's modulus (E, from Refs. 19, 29-31) for each material shown in (a). Homologous temperatures $T_H$ are shown for each curve. The creep resistance of $Mg_{1.96}Al_{0.04}Si_{0.97}Bi_{0.03}$ is similar to that of the various structural silicides shown, but significantly higher than the two previously studied thermoelectric materials $Bi_2Te_3$ (at 500 °C) and PbTe (at 400 °C).

exhibits power-law creep with a stress exponent $n = 7.6 \pm 0.3$, consistent with dislocation creep. No diffusional creep is observed, likely because of a dispersion of ~1 μm Bi-, Al-, and O-rich particles which pin grain boundaries and prevent grain boundary sliding. $Mg_{1.96}Al_{0.04}Si_{0.97}Bi_{0.03}$ exhibits a mixture of brittle and plastic behavior, with the stress and temperature at which catastrophic brittle failure occurs likely dependent on pre-existing flaws in the material. The material creeps at similar stresses when compared to other studied silicides at the same homologous temperature, but exhibits a creep resistance that is much higher than previously-studied thermoelectric materials, PbTe and $Bi_2Te_3$, likely because of the mostly covalent bonding of $Mg_2Si$. This makes $Mg_{1.96}Al_{0.04}Si_{0.97}Bi_{0.03}$ a promising thermoelectric material for power generation systems subjected to particularly high stresses and/or temperatures.

This work made use of the MatCI Facility which receives support from the MRSEC Program (NSF DMR-1121262) of the Materials Research Center at Northwestern University. This work made use of the EPIC facility of Northwestern University's NUANCE Center, which has received support from the MRSEC program (NSF DMR-1121262) at the Materials Research Center; the International Institute for Nanotechnology (IIN); and the State of Illinois, through the IIN. WL thanks the Grant (2017R1A2A1A17069528) and Priority Research Centers Program (2009-0093823) funded by National Research Foundation of Korea (NRF) and Hyundai Motor Company (2016-11-0532).

## References

[1] D.M. Rowe, Renew. Energy 16 (1999) 1251–1256.
[2] J.C. Bass, N.B. Elsner, F.A. Leavitt, AIP Conf. Proc. 316 (1994) 295–298.
[3] E.F. Thacher, B.T. Helenbrook, M.A. Karri, C.J. Richter, Proc. Inst. Mech. Eng. Part J. Automob. Eng. 221 (2007) 95–107.
[4] X. Liu, C.G. Yu, S. Chen, Y.P. Wang, C.Q. Su, J. Electron. Mater. 43 (2014) 2218–2223.
[5] T. Hendricks, W.T. Choate, Engineering Scoping Study of Thermoelectric Generator Systems for Industrial Waste Heat Recovery, Pacific Northwest National Lab. (PNNL), Richland, WA (United States), 2006.

[6] T. Kuroki, K. Kabeya, K. Makino, T. Kajihara, H. Kaibe, H. Hachiuma, H. Matsuno, A. Fujibayashi, J. Electron. Mater. 43 (2014) 2405–2410.
[7] T. Clin, S. Turenne, D. Vasilevskiy, R.A. Masut, J. Electron. Mater. 38 (2009) 994–1001.
[8] A.S. Al-Merbati, B.S. Yilbas, A.Z. Sahin, Appl. Therm. Eng. 50 (2013) 683–692.
[9] G. Kim, J. Kim, H. Lee, S. Cho, I. Lyo, S. Noh, B.-W. Kim, S.W. Kim, K.H. Lee, W. Lee, Scr. Mater. 116 (2016) 11–15.
[10] G. Kim, H. Lee, J. Kim, J.W. Roh, I. Lyo, B.-W. Kim, K.H. Lee, W. Lee, Scr. Mater. 128 (2017) 53–56.
[11] R.G. Morris, R.D. Redin, G.C. Danielson, Phys. Rev. 109 (1958) 1909–1915.
[12] H.J. Frost, M.F. Ashby, Deformation Mechanism Maps: The Plasticity and Creep of Metals and Ceramics, Pergamon Press, Oxford, UK, 1982.
[13] A. Kato, T. Yagi, N. Fukusako, J. Phys. Condens. Matter 21 (2009), 205801. .
[14] M.R. van Buuren, F. Voermans, H. van Kempen, J. Phys. Chem. 99 (1995) 9519–9522.
[15] R.D. Schmidt, E.D. Case, J. Giles, J.E. Ni, T.P. Hogan, J. Electron. Mater. 41 (2012) 1210–1216.
[16] G. Kim, H. Lee, J. Kim, J.W. Roh, I. Lyo, B.-W. Kim, K.H. Lee, W. Lee, Ceram. Int. 43 (2017) 12979–12982.
[17] Z.P. Guan, D.C. Dunand, Mater. Sci. Eng. A 565 (2013) 321–325.
[18] C.C. Li, G.J. Snyder, D.C. Dunand, Scr. Mater. 134 (2017) 71–74.
[19] R. Mitra, Structural Intermetallics and Intermetallic Matrix Composites, CRC Press, 2015.
[20] H. Ishibashi, M. Arita, I. Nishida, A. Yanase, K. Nakahigashi, J. Phys. Condens. Matter 6 (1994) 8681.
[21] H.M. Wang, G. Duan, Mater. Sci. Eng. A 336 (2002) 117–123.
[22] D.M. Shah, D. Berczik, D.L. Anton, R. Hecht, Mater. Sci. Eng. A 155 (1992) 45–57.
[23] R. Rosenkranz, G. Frommeyer, W. Smarsly, Mater. Sci. Eng. A 152 (1992) 288–294.
[24] D.M. Shah, D.L. Anton, Mater. Sci. Eng. A 153 (1992) 402–409.
[25] K. Sadananda, C.R. Feng, R. Mitra, S.C. Deevi, Mater. Sci. Eng. A 261 (1999) 223–238.
[26] P.R. Subramanian, T.A. Parthasarathy, M.G. Mendiratta, D.M. Dimiduk, Scr. Metall. Mater. 32 (1995) 1227–1232.
[27] N.M. Ravindra, V.K. Srivastava, Phys. Status Solidi A 58 (1980) 311–316.
[28] P. Larson, S.D. Mahanti, M.G. Kanatzidis, Phys. Rev. B 61 (2000) 8162–8171.
[29] R.E. Larsen, A.L. Ruoff, J. Appl. Phys. 44 (1973) 1021–1025.
[30] K. Biswas, M.S. Good, K.C. Roberts, M.A. Subramanian, T.J. Hendricks, J. Mater. Res. 26 (2011) 1827–1835.
[31] F. Ren, E.D. Case, J.R. Sootsman, M.G. Kanatzidis, H. Kong, C. Uher, E. Lara-Curzio, R.M. Trejo, Acta Mater. 56 (2008) 5954–5963.